Excitation Wavelength Dependent and Auxiliary-Ligand Tuned Intersystem Crossing Efficiency in Cyclometalated Platinum(II) Complexes: Spectroscopic and Theoretical Studies

Kai Li,[†,‡] Glenna So Ming Tong,*[,†] Jia Yuan,[§] Chensheng Ma,[†] Lili Du,[†] Chen Yang,[†] Wai-Ming Kwok,[∥] David Lee Phillips,[†] and Chi-Ming Che*[,†,#]

[†]State Key Laboratory of Synthetic Chemistry, Department of Chemistry, The University of Hong Kong, Pokfulam Road, Hong Kong, People's Republic of China

[‡]Shenzhen Key Laboratory of Polymer Science and Technology, College of Materials Science and Engineering, Shenzhen University, Shenzhen 518055, People's Republic of China

[§]Key Laboratory of Pesticide & Chemical Biology, Ministry of Education, and Chemical Biology Center, College of Chemistry, Central China Normal University, Wuhan 430079, People's Republic of China

[∥]Department of Applied Biology and Chemical Technology, The Hong Kong Polytechnic University, Hung Hom, Kowloon, Hong Kong, People's Republic of China

[#]HKU Shenzhen Institute of Research and Innovation, Shenzhen, People's Republic of China

ABSTRACT: Understanding the factors affecting the ISC rate constant (k_{ISC}) of transition metal complexes is crucial to material design with tailored photophysical properties. Most of the works on ISC to date focused on the influence by the chromophoric ligand and the understanding of ISC efficiency were mainly drawn from steady-state fluorescence to phosphorescence intensity ratio and ground state calculations with only a few high-level calculations on k_{ISC} that take excited state structural change and solvent reorganization into account for quantitative comparisons with experimental data. In this work, a series of $[Pt(thpy)X)]^+$ complexes were prepared (Hthpy = 2-(2'-thienyl)pyridine; X = auxiliary ligands) and characterized by both steady-state and time-resolved luminescence spectroscopies. A panel of auxiliary ligands with varying σ-donating/π-accepting characters have been used. For comparison, analogues of $[Pt(ppy)(P\hat{}P)]^+$ (Hppy = 2-phenylpyridine, P^P = diphosphino ligand) were also examined. The $[Pt(thpy)(P\hat{}P)]^+$ complexes exhibit dual fluorescence-phosphorescence emissions with their ISC rate constants varied with the electronic characteristics of the auxiliary ligand: the more electron-donating ligand induces faster ISC from the S_1 excited state to the triplet manifolds. DFT/TDDFT calculations of the $k_{ISC}(S_1 \rightarrow T_2)$ at the optimized excited state geometries give excellent quantitative agreement with the femtosecond time-resolved fluorescence measurements; it was revealed that the more electron-donating auxiliary ligand increases metal contributions to both occupied and virtual orbitals and decreases the energy gap of the coupling excited states, leading to a decrease in activation energy and an increase in spin-orbit coupling (SOC). Furthermore, the ISC rate constants of $[Pt(thpy)(P\hat{}P)]^+$ complexes are found to depend on excitation wavelengths. The deviation from Kasha-Vavilov's rule upon photo-excitation at $\lambda_{exc} < 350$ nm is due to the ultrafast $S_2 \rightarrow T_2$ and $S_2 \rightarrow T_3$ ISC as demonstrated by the calculated $\tau_{ISC} < 100$ fs, giving hints as to why $S_2 \rightarrow S_1$ internal conversion ($\tau_{IC} \sim$ ps) is not competitive with this hyper intersystem crossing.

INTRODUCTION

Singlet and triplet excited states exhibit different photophysical and photochemical properties. For example, the natural radiative lifetime (τ_r) of a triplet excited state is usually on the microsecond timescale for transition metal complexes and could exceed 1 s for pure organic compounds, whereas τ_r of a singlet excited state is on the nanosecond regime. As singlet excited states are usually short-lived, they have relatively little chemistry of their own particularly with regard to bi-molecular reactions. On the contrary, triplet excited states are generally long-lived and thus display rich photo-chemistry. Moreover, phosphorescence is generally more sensitive to local environment and is therefore highly responsive to the presence of quenchers. Therefore, molecules that display dual fluorescence-phosphorescence at ambient temperature are potential candidates of luminescent ratiometric sensory materials.[1-8] In general, upon photo-excitation, singlet excited states are populated because this is a spin-allowed process; triplet excited states are, on the other hand, usually formed via intersystem crossing (ISC) from a singlet excited state after photo-excitation. Depending on the singlet→triplet ISC efficiency (with rate constant k_{ISC}), the molecule would display (1) steady state fluorescence if $k_f >> k_{ISC}$ (k_f = singlet

decay rate constant), (2) phosphorescence if $k_{ISC} >> k_f$ and there are no efficient deactivation channels for triplet radiative decay, and (3) dual fluorescence-phosphorescence if k_f and k_{ISC} are of comparable magnitudes. Therefore, understanding the factors governing the ISC rate is crucial to the tailoring of emission properties of transition metal complexes.

Normally, ISC is expected in regions of near resonance and non-zero spin-orbit coupling (SOC) between the singlet and triplet excited states. As such, larger SOC and smaller singlet-triplet energy gap would lead to a faster ISC rate. Incorporation of heavy atom(s) in the molecule is a straightforward way to increase SOC due to "heavy atom effect". However, there are a number of literature reports revealing that there may not be direct correlation between the ISC rates and SOC constants.[9-24] Rather, the nature of ligand(s) coordinated to the metal ion appears to play a more decisive role in determining the ISC rate. For instance, Vlček and co-workers demonstrated that changing the chromophoric ligand L in $[ReCl(CO)_3L]$ from phen or bpy to impy (phen = phenanthroline, bpy = bipyridine, and impy = 1-(2-pyridyl)-imidazo[1,5-α]pyridine) slows down the ISC rate by a factor of 200–300.[25] We and Chou independently reported that increasing the chain length *n* of oligophenylacetylene $(C\equiv C\text{-}1,4\text{-}Ph)_n$ and oligophenylene $(1,4\text{-}Ph)_n$ respectively in the corresponding Au(I) complexes could lead to a decrease in ISC rate by about 4 orders of magnitude.[26-30] In addition, the ISC dynamics also depends on the substitution pattern of the oligophenylacetylene (*meta*- vs *para*-). We previously reported a theoretical basis of how changing the bridging ligand of a tetragold(I) complex from ethylene to phenyl could switch its luminescence from fluorescence to phosphorescence.[13] However, all these works were focused on the effect of the chromophoric ligand on the ISC rate. There are, to the best of our knowledge, only few reports which explicitly address the effect of an auxiliary ligand on the ISC efficiency. Herein the auxiliary ligand is referred to as a ligand that is not directly involved in the emissive excited state(s) (i.e., orbitals involved in the emissive excited state have little or no contributions from the auxiliary ligands). Karttunen, Chou, and Koshevoy reported that increasing the electron-donating characteristics of the alkynyl auxiliary ligand of a family of dinuclear gold(I) diphosphine complexes enhanced the participation of metal dπ and alkynyl orbitals to the S_1 excited state and inferred this to be the cause of the corresponding increase in k_{ISC}.[6] Winter *et. al.* showed that the intensity ratio of the phosphorescence to fluorescence varies with the auxiliary anionic ligand X in *trans*-$Pt(BODIPY)X(PEt_3)_2$ (BODIPY = 4,4-difluoro-4-bora-3*a*,4*a*-diaza-*s*-indacen-8-yl); X = Cl, I, NO_2, NCS, CH_3) and the ratio parallels the *trans*-influence of the ligand X.[5] They have also found that replacing the PEt_3 ligands with PPh_3 ligands in *trans*-$Pt(BODIPY)Br(PEt_3)_2$ gives rise to retarded $S_1 \rightarrow T_1$ ISC as reflected by the higher fluorescence quantum yield in the PPh_3 complex than in the PEt_3 analogue.[4] However, in these reports, neither the ISC rates for the $Pt(BODIPY)X(PEt_3)_2$ complexes have been determined from time-resolved measurements nor detailed calculations on ISC rate constants have been performed to delineate the factors that modulate the ISC efficiency. As research on dual fluorescence-phosphorescence has been gaining momentum, it would be of profound interest to use more rigorous approach to figure out how changing the nature of an auxiliary ligand would affect ISC efficiency and hence, the relative fluorescence-to-phosphorescence intensities, without significantly altering the energies of the emissive singlet and triplet excited states. In the literature, Gray[31] and Chergui[32] reported studies on the excited state dynamics of intersystem crossing of a diplatinum(II,II) complex; nonetheless, systematic investigation of the role of auxiliary ligand in tuning the ISC and a direct comparison between experimental and calculated results have not yet performed.

It is known that SOC between ^{1,3}MLCT states (MLCT = metal-to-ligand charge transfer) is effective and leads to large zero-field splitting (zfs) and facile ISC (in the fs regime).[33] But when the singlet and/or triplet excited states have more IL character (IL = intraligand), SOC would become smaller, giving rise to smaller zfs and slower ISC rate. In the literature, the emissive triplet excited state of the Pt(II) complexes supported by substituted thienylpyridine ligands have been found to be largely ligand-centered and thus spin-orbit coupling between the T_1 excited state and singlet excited states are expected to be not large, as revealed by low-temperature high-resolution luminescence studies with zfs < 20 cm^{-1}.[34] Inclusion of additional thienyl rings further induces a slowdown of $S_1 \rightarrow T_1$ ISC and results in the dual fluorescence/phosphorescence emission.[2,35] Notably, the $S_1 \rightarrow T_1$ ISC rate constants for substituted [Pt(thpy)(acac)] (acac = deprotonated acetylacetone) complexes were estimated to be 2 orders of magnitude smaller than that of the [Pt(ppy)(acac)] analogues (Hppy = 2-phenylpyridine).[20] These findings convinced us that $[Pt(thpy)X]^+$ complexes, the subject of the present study, offer a possibility to systematically investigate the ISC efficiency by varying the auxiliary ligand X from a π-accepting bis(di-R-phosphino)alkane (P^P) ligand (R = electron-donating cyclohexyl or electron-withdrawing phenyl; Figure 1) to a σ-donating *bis*-carbene (NHC) one. In this article, the effect of P^P ligand on the ISC rates and the luminescence properties of $[Pt(thpy)(P\text{^}P)]^+$ complexes, **Pt1**–**Pt9**, was investigated. The combined spectroscopic and DFT/TDDFT analyses allow one to characterize the pathways that lead to different photo-physical behavior, *viz.*, fluorescence only, dual fluorescence-phosphorescence, or phosphorescence only. The photophysical studies of the $[Pt(thpy)(bis\text{-}NHC)]^+$ and $[Pt(ppy)(P\text{^}P)]^+$ (Hppy = 2-phenylpyridine) analogues, **Pt10**–**Pt14**, were also performed for comparisons.

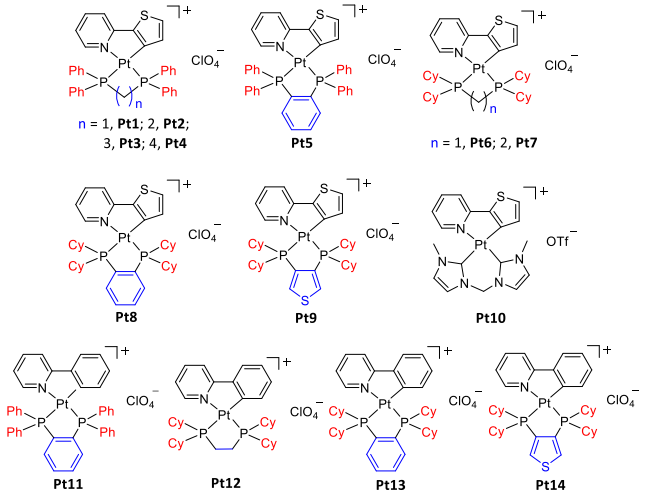

Figure 1. Chemical Structures of the $[Pt(thpy)X]^+$ and $[Pt(ppy)(P\hat{}P)]^+$ complexes.

RESULTS AND DISCUSSION

Synthesis and Structures. Reaction of $[Pt(thpy)(Hthpy)Cl]$[36] with a panel of diphenyl- or dicyclohexylphosphino ligands (P^P) in 1:1 molar equivalent in acetonitrile afforded $[Pt(thpy)(P\hat{}P)]^+$ complexes, **Pt1**–**Pt9**, which were precipitated as perchlorate salts upon addition of $LiClO_4$ and obtained in moderately good yields (50–76 %). The complexes **Pt11**–**Pt14**, were prepared using a similar procedure but from dinuclear (μ-chloro) complex $[Pt(ppy)(\mu\text{-}Cl)]_2$. The synthesis of **Pt10** has been reported previously.[37] All complexes were characterized by multinuclear (^1H, ^{13}C and ^{31}P) NMR spectroscopy, FAB or high-resolution mass spectrometry (HRMS), and satisfactory elemental analyses. The synthetic procedures and characterization data for all complexes are given in the SI. These complexes are air- and moisture-stable at room temperature in solid state.

Single crystals of the $[Pt(thpy)(P\hat{}P)](ClO_4)$ complexes **Pt1**–**Pt9** and $[Pt(ppy)(P\hat{}P)](ClO_4)$ complexes **Pt11**–**Pt13** were obtained by slow diffusion of diethyl ether into acetonitrile solutions. The crystal data with selected bond lengths and angles are given in SI (Table S1–S2). The ORTEP diagrams with P–Pt–P bite angle of **Pt1**–**Pt4** are depicted in Figure 2. The platinum atom resides in an approximately square planar coordination environment. The Pt–N and Pt–C bond distance and the N–Pt–C bite angle of the $[Pt(thpy)]^+$ moiety are *ca.* 2.1 Å, 2.1 Å, and 80°, respectively. The P–Pt–P bite angle of the complexes **Pt1**–**Pt4** increases with the number of methylene spacers n: 73.13° (n = 1; **Pt1**) < 85.53° (n = 2; **Pt2**) < 92.50° (n = 3; **Pt3**) < 96.34° (n = 4; **Pt4**).[38] Complex **Pt6**, having the same number of CH_2 units in the diphosphine ligand as **Pt1**, has a P–Pt–P bite angle (∠P–Pt–P = 73.77/73.84°) very close to that in the analogue **Pt1** (Figure S1). Similarly, the bite angles in **Pt2**, **Pt5**, **Pt7**–**Pt9**, and **Pt11**–**Pt13** which have a 5-membered metallocycle, are in the narrow range of 83.75–87.65°, revealing that the bite angle is mainly determined by the ring size.[39,40] No close Pt–Pt or π–π contact is noted in the crystal structures, probably due to the presence of sterically bulky diphosphine ligands.

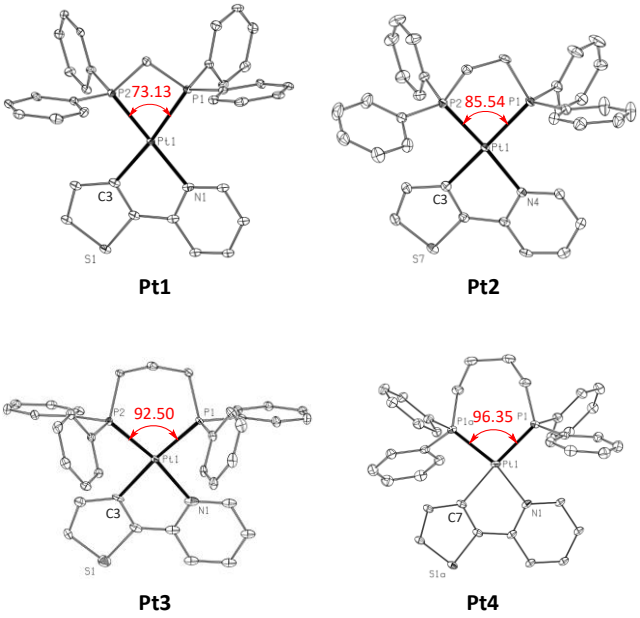

Figure 2. Single crystal X-ray structures of **Pt1**–**Pt4** showing the tuned bite angle by varying the number of methylene units (H atoms have been omitted for clarity).

Electronic Absorption. Figure 3 displays the electronic spectra of complexes **Pt1**–**Pt10** in acetonitrile (MeCN) solution at room temperature. All complexes show intense vibronically structured absorption at 250–325 nm with molar absorptivity on the order of 10^4 M^{-1} cm^{-1} which are attributed to ligand-centered transition from S_o states to high-lying electronic states (S_n, n>1). The less intense, structureless, broad absorption bands at 350–430 nm with maxima molar absorptivity of 3–5 × 10^3 M^{-1} cm^{-1} are assigned to $S_o \rightarrow S_1$ transition. The low energy absorption peak maxima (λ_{max}) for the $[Pt(thpy)(P\hat{}P)]^+$ complexes at ca. 389–403 nm span only a small range of 893 cm^{-1} upon varying the auxiliary P^P ligand. This is attributed to the fact that this lowest absorption peak, being derived from the S_1 excited state, is assigned to a dominantly thpy-localized intraligand $^1\pi$-π^* transition. This assignment is supported by the minor solvatochromic effect (3–10 nm) on this lowest absorption peak upon changing the solvent from acetonitrile to dichloromethane. The absorption of **Pt10**, which bears the auxiliary carbene ligand, lies at a similar regime, thus further reveals that the ancillary ligand has little character in the orbitals involved in this transition. In contrast, the lowest-energy absorption of the $[Pt(ppy)(P\hat{}P)]$ analogues, **Pt11**–**Pt14**, are blue-shifted (< 400 nm) and are assigned to phenylpyridyl ligand-localized $^1\pi$-π^* transition (Figure S2 in the SI). Such blue shifts are likely due to the lower-lying HOMOs which are localized on the phenyl moiety in comparison to that on the thiophene moiety in **Pt1**–**Pt10** (as an example, see Figure S18 and S19 in SI).

Table 1 Photophysical data of $[Pt(thpy)X]^+$ complexes[a]

	Medium (T/K)	Absorption λ_{abs} / nm (ε / 10^3 $M^{-1}cm^{-1}$)	Fluorescence λ_{max} / nm (τ / ps)[b]	Phosphorescence λ_{max} / nm (τ / μs)[c]	Φ_{em}[d]
Pt1	CH_3CN (298)	267 (22.0), 275 (20.2), 297 (sh, 12.5), 316 (sh, 10.1), 397 (3.60)	454 (167)	564 (2.0), 605	4.6×10^{-3}
	PMMA (298)		456	560 (35.3), 603	0.31
	Glass (77)		456	554 (59.8), 599	
	Solid (298)		487	583 (32.4), 602	
	Solid (77)		476	554, 583 (55.2), 596, 634	
Pt2	CH_3CN (298)	260 (sh, 19.8), 266 (sh, 19.0), 273 (17.0), 299 (11.3), 393 (3.96)	454 (165)	558 (2.2), 598	4.4×10^{-3}
	PMMA (298)		449	554 (41.4), 596	0.25
	Glass (77)		447	548 (70.4), 594	
	Solid (298)		463	575, 601 (35.3)	
	Solid (77)		454	563 (46.2), 601	
Pt3	CH_3CN (298)	266 (sh, 15.7), 274 (14.4), 299 (10.8), 322 (7.65), 389 (4.15)	448 (42.6)	551 (–)	1.1×10^{-3}
	PMMA (298)		446	551 (43.4), 592	0.19
	Glass (77)		442	545 (76.1), 591	
	Solid (298)		459	569, 597 (45.7)	
	Solid (77)		457	549 (44.5), 597, 608	
Pt4	CH_3CN (298)	265 (sh, 16.5), 274 (15.0), 299 (11.4), 320 (sh, 8.25), 390 (4.42)	446 (107)	553 (1.6) 594	6.0×10^{-4}
	PMMA (298)		448	552 (39.2), 594	0.14
	Glass (77)		444	541 (104.9), 585	
	Solid (298)		481	564, 599 (2.1, 10.7)	
	Solid (77)		470	559 (39.3), 605	
Pt5	CH_3CN (298)	269 (sh, 20.6), 299 (12.3), 317 (9.61), 393 (3.90)	454	555 (1.9), 599	4.3×10^{-3}
	PMMA (298)		449	556 (41.3), 596	0.26
	Glass (77)		447	549 (76.9), 597	
	Solid (298)		477	575 (15.0), 606	
	Solid (77)		–[e]	575 (54.2), 626	
Pt6	CH_3CN (298)	256 (14.6), 281 (15.5), 300 (sh, 11.8), 317 (sh, 9.70), 394 (3.80)	459 (87.4)	561 (10.0), 602	1.2×10^{-2}
	PMMA (298)		451	558 (32.4), 599	0.25
	Glass (77)		448	552 (47.9), 598	
	Solid (298)		470	564 (19.2), 609	
	Solid (77)		482	564 (30.9), 611	
Pt7	CH_3CN (298)	261 (10.7), 278 (13.2), 301 (10.9), 317 (8.63), 389 (4.10)	452	553 (0.4), 594	2.6×10^{-3}
	PMMA (298)		444	552 (35.0), 592	0.28
	Glass (77)		445	548 (59.7), 595	
	Solid (298)		466	572 (40.2), 600	
	Solid (77)		465	572 (55.2), 623	
Pt8	CH_3CN (298)	264 (sh, 12.4), 273 (12.8), 318 (8.05), 393 (3.87)	453	556 (11.7), 600	1.2×10^{-3}
	PMMA (298)		446	555 (36.0), 592	0.17
	Glass (77)		448	550 (76.4), 596	
	Solid (298)		464	568 (8.3, 1.5), 609	

	Solid (77)		468	568 (38.3), 619	
Pt9	CH_3CN (298)	261 (15.7), 277 (14.2), 301 (11.9), 317 (9.89), 389 (4.60)	453	556 (22.6), 600	6.8×10^{-3}
	PMMA (298)		445	554 (33.3), 594	0.23
	Glass (77)		445	551 (68.4), 595	
	Solid (298)		471	583 (11.8, 2.3), 612	
	Solid (77)		463	577 (43.9), 627	
Pt10	CH_3CN (298)	278 (20.8), 297 (sh, 17.4), 308 (sh, 14.6), 330 (11.6), 397 (2.95)	–[e]	559 (26.8), 601	0.08
	Glass (77)		–[e]	552 (30.0), 600	
	Solid (298)		–[e]	580 (0.8), 606	
	Solid (77)		–[e]	573 (14.8), 624	
Pt11	CH_3CN (298)	269 (24.7), 319 (5.64), 328 (5.61), 360 (brd, 2.29)	–[e]	–[e]	
	PMMA		–[e]	477 (32.4), 510	0.24
	Glass (77)		–[e]	472 (64.0), 507, 537 (sh)	
	Solid (298)		–[e]	478 (20.1), 513, 544 (sh)	
	Solid (77)		–[e]	479 (31.1), 516, 546 (sh)	

[a]Excitation wavelength at 390–400 nm for all measurements. The glass emissions were measured in 77 K butyronitrile. [b]Determined from fs time-resolved emission spectra (error = ±3%). [c]Determined using a Quanta Ray GCR 150-10 pulsed Nd:YAG laser system with 355 nm output. [d]Photoluminescence quantum yield (PLQY) for solution was estimated with reference to quinine sulphate in 0.1 M H_2SO_4 (Φ = 0.546). PLQY for thin film sample was measured using Hamamatsu C11347 Quantaurus-QY Absolute PL quantum yields measurement system. The error for PLQY measurement is ±10%. [e]weak or not observed.

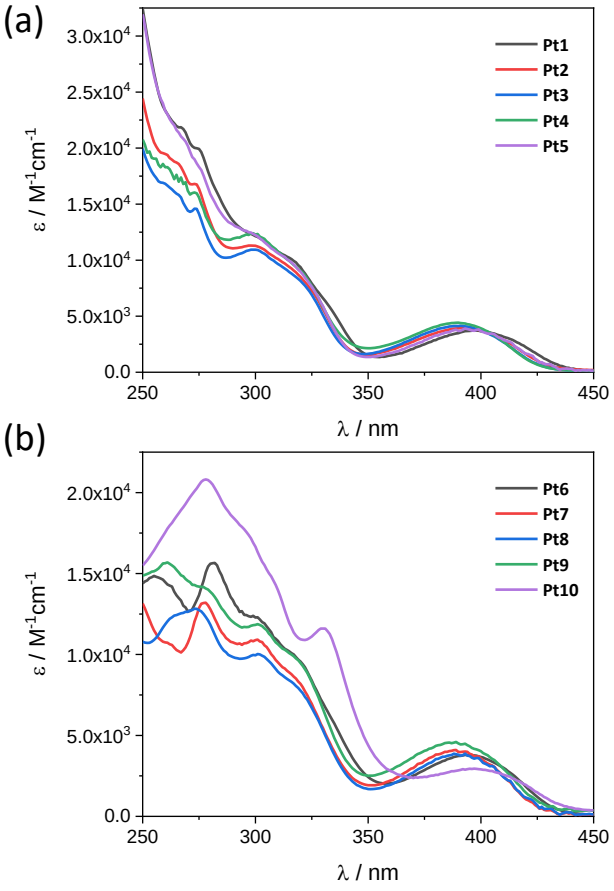

Figure 3. UV-visible absorption spectra of (a) **Pt1**–**Pt5** and (b) **Pt6**–**Pt10** in acetonitrile at room temperature (concentration = 4×10^{-5} M).

Excitation Dependent Dual Fluorescence-Phosphorescence Emission. The photoluminescent properties of all complexes in various states have been examined. First, the steady-state emission of the [Pt(thpy)(P^P)] complexes **Pt1**–**Pt9** show interesting features. As shown in Figure 4 and Figure S3–S11, all [Pt(thpy)(P^P)] complexes show dual emission comprising a high-energy (HE), broad band at λ_{max} = 466–473 nm and a low-energy (LE), vibronic structured band at λ_{max} = 558–564 nm in solutions at room temperature. The steady state emission spectra show that both the HE and LE emission peak maxima do not shift significantly upon varying the auxiliary ligand (~318 cm^{-1} for the HE peak and ~191 cm^{-1} for the LE peak). The presence of trace amount of strongly emissive impurity that may give rise to the HE emission has been excluded on the basis of reproducible dual HE and LE emission bands observed for different batches of samples including those from single crystals. In addition, the excitation spectra at the HE and LE emission maxima for **Pt1**–**Pt9** match well with their absorption in the low energy region, showing that these two emitting states share the same origin that absorbs the photo-excitation.

Information regarding the nature of these two emitting states were gained by time-resolved photoluminescence studies. The lifetimes of LE emission lie in the microsecond regime (2–29 μs, Table 1) in degassed solutions. In aerated solutions, the LE emission bands are drastically quenched (Figure 4c and Figure S3–S11). The LE emission bands are assigned to phosphorescence from T_1 states. On the other hand, the HE emission bands are insensitive to molecular oxygen. The femtosecond time-resolved fluorescence spectroscopy (fs-TRF) of **Pt1**–**Pt4** and **Pt6** show emission bands

at ca. 460 nm with decay constants of 43–167 ps (Table 1 and Figure 4d). Thus, the HE emission bands for **Pt1**–**Pt9** are ascribed to fluorescence. Comparing to the ultrafast decay of fluorescence for many other Pt(II) complexes (<1 ps),[41-43] the much longer fluorescence lifetimes of the present complexes reveal significantly retarded ISC which are estimated to be on the order of 10^{10} s^{-1}.

Another important feature associated with the dual fluorescence/phosphorescence property is the excitation wavelength dependence of the relative intensity of the LE to HE emission band for each complex (Figure 4a and Figure S3–S11); short wavelength excitation favors the LE emission. The excitation spectra monitored at both the HE and LE bands also reveal that short wavelength absorption leads to dominant phosphorescence. These properties are reminiscent of Os(II) and Ag(I) complexes reported by Chi, Chou and co-workers which show excitation wavelength-dependent dual fluorescence-phosphorescence emission behavior.[15] Accordingly, it is postulated that such a behavior for the present Pt(II) complexes is a result of the inter-system crossing from higher-lying singlet excited state to triplet excited state, i.e., hyper inter-system crossing (HISC). Although there are a handful of Pt(II) complexes exhibiting dual fluorescence/phosphorescence due to inefficient ISC, the present type complexes is one of the few reports on HISC for Pt(II) emitters.[20] The photophysical properties of **Pt1**–**4** and **Pt6** in dichloromethane have also been examined and they show similar dual fluorescence/phosphorescence behavior (Figure S12 in the SI). Whereas, the carbene-bearing **Pt10** shows only dominant phosphorescence in both acetonitrile and dichloromethane. All of the [Pt(thpy)(P^P)] complexes **Pt1**–**Pt9** in thin film (5 wt% in PMMA), solid state (298 K and 77 K), and glassy solution (77 K) exhibit dual fluorescence/phosphorescence emission behavior with the relative intensity ratio dependent on the local environment (rigidity and temperature etc.). In contrast, when the chromophore ligand is changed to phenylpyridine as that in **Pt11**–**Pt14**, these complexes become non-emissive in solutions at room temperature. Only one dominant vibronic structured band that is attributable to phosphorescence is observed for these complexes in other condensed phases (Figure S13). The predominant phosphorescent emission for this series of complexes is probably due to the higher metal character of HOMO and the close-lying triplet excited state which facilitate SOC between S_1 and triplet state (vide infra, the calculation) and thus faster ISC process. Fs-time resolved spectroscopic measurements revealed ISC < 1 ps (Figure S14).

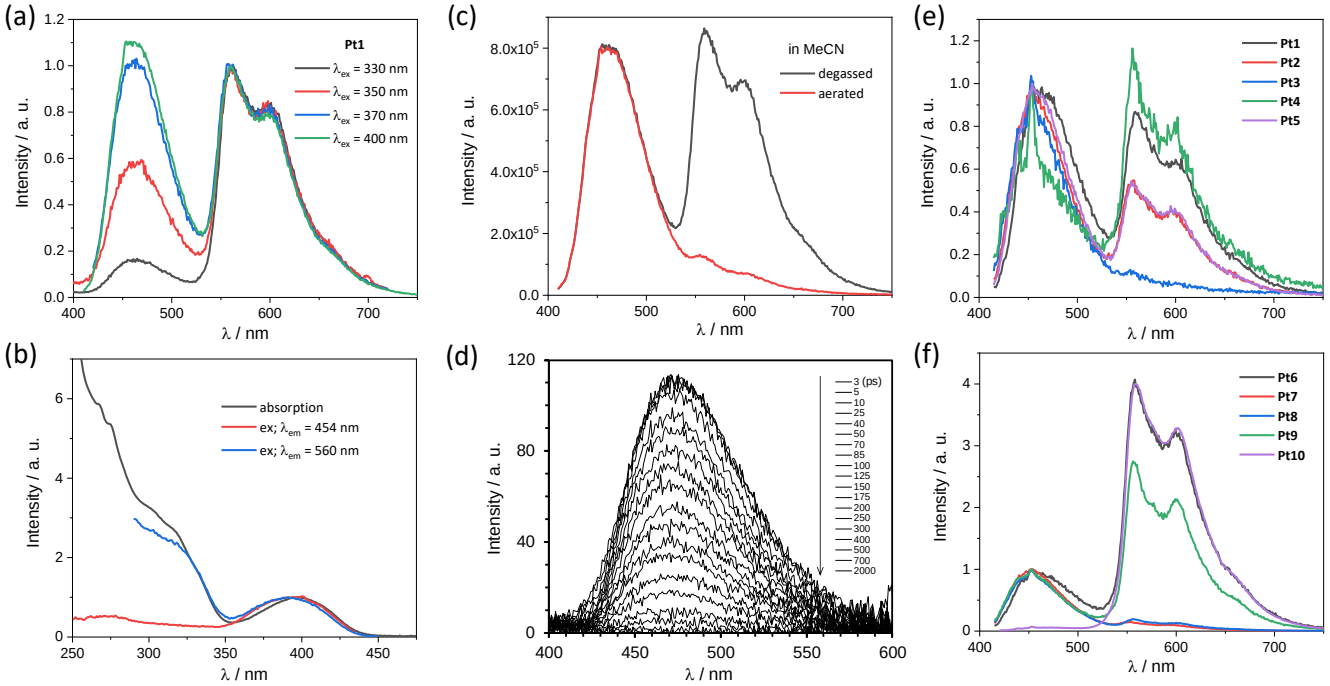

Figure 4. (a) Normalized emission spectra of **Pt1** in degassed acetonitrile at different excitation wavelengths (concentration = 4×10^{-5} M). (b) Comparison of the normalized UV-vis absorption and excitation spectra monitored at different emission wavelengths for **Pt1**. (c) Comparison of the emission spectra of **Pt1** in the absence and presence of oxygen. (d) fs-TRF spectra of **Pt1** in acetonitrile upon excitation at 390 nm. Normalized emission spectra of (e) **Pt1**–**Pt5** and (f) **Pt6**–**Pt10** in degassed acetonitrile (concentration = 4×10^{-5} M; λ_{ex} = 400 nm).

Auxiliary Ligand-Dependent Intersystem Crossing Rate. Altering the auxiliary ligand of $[Pt(thpy)X]^+$ does not change the emission energy considerably but results in very different relative intensities of the phosphorescence (LE) to fluorescence (HE) emission. Specifically, the series **Pt1**–**Pt5** which bear $Ph_2P\text{^}PPh_2$ auxiliary ligand, show discernible HE and LE emission bands, except **Pt3** where only the HE peak is conspicuous (Figure 4e); for the dicyclohexyl analogues, **Pt7** and **Pt8** exhibit predominant HE emission while **Pt6** and **Pt9** display both HE and LE dual-

emissions with the latter pair having higher intensities (Figure 4f). When the auxiliary ligand is a strong σ-donating *bis*-NHC (**Pt10**), the LE emission is predominant and HE emission is barely observed. Manipulation of the ISC rate through changing auxiliary ligand is inferred as the key to achieving dual fluorescence/phosphorescence emission. Tuning of radiative and non-radiative rates of S_1 and T_1 states through synthesis and molecular design has been the major focus for the development of fluorescent and phosphorescent emitters, respectively. Nevertheless, systematic studies on the dual fluorescence/phosphorescence metal complexes, in particular on the unique HISC shown in this work, are sparse.

Calculations on [Pt(thpy)X]$^+$ Complexes at The Optimized Ground State Geometries. To shed light on the interesting photo-physics of this series of complexes, first principle methods were applied to study the excited state decay rates of selected [Pt(thpy)X]$^+$ complexes, *viz.*, X = dppm (**Pt1**), dcpm (**Pt6**), and (*bis*-NHC) (**Pt10**). These complexes are chosen with the following objectives: (a) how does varying the nature of substituent of the P^P auxiliary ligand change the ISC rate and thus the relative intensities of the fluorescence to phosphorescence of [Pt(thpy)(P^P)]$^+$ complexes? (b) why does changing the auxiliary ligand from a π-accepting phosphine ligand to a σ-donating carbene ligand results in dominant phosphorescence for the [Pt(thpy)(*bis*-NHC)]$^+$ complex, and hence, what is the reason for the enhanced ISC efficiency in [Pt(thpy)(*bis*-NHC)]$^+$?

As aforementioned, ISC is facile when singlet-triplet energy gap is small and SOC is large. In the literature, most often these two parameters were compared among the studied complexes at *the ground state* geometries. Thus, we first present the data at the DFT-optimized ground state geometries. Table S3 (SI) lists the low-lying singlet and triplet excited state energies and their nature. The $S_0 \rightarrow S_1$ excitation energies, calculated to be at 382–400 nm (Table S3), are in good agreement with the experimental lowest absorption peaks (< 500 cm^{-1} difference, see also Figure S15 for the simulated absorption spectra). The S_1 excited state, as revealed from TDDFT calculations, is derived mainly from a HOMO→LUMO transition for all the complexes studied. Both the HOMO and LUMO are composed primarily of π(thpy) character with some contributions (< 12%) from Pt; there is only a minute contribution of the auxiliary ligand X to the HOMO (< 3%) and LUMO (< 13%) for all complexes studied (see Figure 5 and Figure S16 for the MO surfaces of complex **Pt1**; other complexes have similar MO surfaces unless otherwise stated). Therefore, the lowest energy absorption peaks of [Pt(thpy)X]$^+$, being best described as a $^1\pi\pi^*$(thpy) IL excited state mixed with some ^{1}MLCT (^{1}[dπ(Pt)→π*(thpy)]) character, have similar S_1 absorption energies. The next singlet excited state, S_2, is found to be at λ_{abs} < 340 nm from TDDFT calculations at the optimized ground state geometries and hence, excitation at λ_{exc} > 380 nm should populate only the S_1 excited state. Thus, in what follows, we only consider triplet excited states close to S_1 and assume that the ISC takes place from the S_1 excited state.

Figure 5. Frontier molecular orbital (FMO) surfaces of **Pt1** in S_1 state at the optimized S_0 geometry. The values in the parenthesis indicate the % contribution of Pt.

Table S4 in the Supporting Information presents the S_1–T_n energy gaps and the corresponding spin-orbit coupling matrix elements between the S_1 and T_n excited states at the respective optimized S_0 geometries. Usually, it is presumed that ISC proceeds from $S_1 \rightarrow T_1$, thus, we first look at this ISC pathway (the first row in Table S4 in SI). The calculated S_1–T_1 energy gap is in the ascending order X = *bis*-NHC (6569 cm^{-1}) < dcpm (6882 cm^{-1}) ~ dppm (6897 cm^{-1}). However, experimental photo-physical data depicted in Table 1 (relative fluorescence-phosphorescence intensities and time-resolved fluorescence lifetimes) implies that the ISC efficiency is likely in the order X = *bis*-NHC > X = dcpm > X = dppm. *Thus, a correlation between S_1–T_1 energy gap estimated at the ground state geometry and ISC rate cannot be made for the [Pt(thpy)X]$^+$ complexes*.

Although T_2 and T_3 excited states are higher-lying than the S_1 excited state at the ground state geometries by more than 1000 cm^{-1}, the S_1–T_2 and S_1–T_3 energy gaps are much smaller than the S_1–T_1 energy gap (Table S4 in SI). Moreover, the SOC matrix elements (H_{SOC}) between S_1 and T_n (n = 2 or 3) are one to two orders of magnitude larger than those between S_1 and T_1. Since $k_{ISC} \propto H_{SOC}^2$, the ISC rates of $S_1 \rightarrow T_2$ and $S_1 \rightarrow T_3$ should be two to four orders of magnitude faster than that of $S_1 \rightarrow T_1$ if we solely consider the electronic factor of H_{SOC}. Therefore, it is speculated that ISC from S_1 to T_2 or T_3 excited state may be more efficient than to the T_1 excited state.

Calculated ISC Rates from $S_1 \rightarrow T_n$ (n = 1–3). To gain further insight into the ISC efficiency of these [Pt(thpy)X]$^+$ complexes, we calculated the ISC rate of $S_1 \rightarrow T_n$ (n = 1, 2, and 3) at the *optimized excited state* geometries for **Pt1**, **Pt6**, and **Pt10**. According to the Fermi Golden Rule under the Condon approximation, the ISC rate is given by the following equation:[44]

$$k_{ISC} = \frac{2\pi}{\hbar} V^2 (\mathrm{FCWD}) \qquad (1)$$

V is the electronic factor and in the present study, it is taken to be the direct SOC matrix element between the S_1 and T_n excited states ($\langle S_1|H_{SOC}|T_n\rangle$). FCWD is the Franck-Condon weighed density and it is related to the structural change and the energy difference between the potential energy minima of the coupling singlet and triplet excited states. In the high-temperature limit,[45-47]

$$FCWD = \frac{1}{\sqrt{4\pi\lambda k_B T}} exp\left[-\frac{(\Delta E+\lambda)^2}{4\lambda k_B T}\right] \quad (2)$$

ΔE is the adiabatic energy difference between the triplet (T_n) excited state and the singlet (S_1) excited state involved in the ISC process at their respective optimized excited state geometries:

$$\Delta E = E^{Tn}(Q_0^{Tn}) - E^{S1}(Q_0^{S1}) \quad (3)$$

Here, $E^{ES}(Q_o^{ES})$ is the energy of the excited state (ES) at the optimized excited state geometry (Q_o^{ES}). λ is the reorganization energy (a measure of the structural change between the coupling excited states) and, because we have used a state-specific approach (i.e., SS-PCM) to compute the $E^{ES}(Q_o^{ES})$, both the intramolecular and solvent reorientation components are included:

$$\lambda = E^{S1}(Q_0^{Tn}) - E^{S1}(Q_0^{S1}) \quad (4)$$

$E^{S_1}(Q_o^{Tn})$ and $E^{S_1}(Q_o^{S_1})$ are the first singlet (S_1) excited state energies at respectively the optimized T_n and S_1 excited state geometries. k_B is the Boltzmann constant and T is temperature (in K).

Table 2 gives the energy difference (ΔE), reorganization energy (λ), and H_{SOC}^2 between the S_1 and T_n excited states. Table 3 presents the $S_1 \rightarrow T_n$ ISC rate constants (k_{ISC}) and the $S_1 \rightarrow S_0$ radiative decay rate constants (k_f) obtained from calculations. These theoretical results are all computed with the Pt(II) complex in acetonitrile; for analogous results in dichloromethane, see Table S5 and S6 in the SI.

Table 2 S_1–T_n energy gaps, ΔE (eV), reorganization energies, λ (eV), and the associated SOC matrix element $\langle S_1|H_{SOC}|T_n\rangle^2$ (cm^{-2}) of $[Pt(thpy)X]^+$ complexes for $S_1 \rightarrow T_n$ ISC obtained at the optimized excited state geometries. All values listed are computed in acetonitrile except $[Pt(thpy)(bis\text{-NHC})]^+$ complex[a,b]

	X = dppm (**Pt1**)			X=dcpm (**Pt6**)			X = *bis*-NHC (**Pt10**)[b]		
n	ΔE	λ	$\langle S_1\|H_{SOC}\|T_n\rangle^2$	ΔE	λ	$\langle S_1\|H_{SOC}\|T_n\rangle^2$	ΔE	λ	$\langle S_1\|H_{SOC}\|T_n\rangle^2$
1	-0.77	0.16	2.71	-0.75	0.17	14.23	-0.75	0.16	19.33
2	-0.04	0.29	92.60	-0.05	0.28	3.59×10^2	-0.05	0.27	1.66×10^3
3	+0.16	0.13	3.78×10^3	+0.20	0.11	2.57×10^4	+0.23	0.11	2.86×10^4

[a]The energies reported here are obtained using a state-specific approach (SS-PCM), see SI for computational details. [b]The values for the $[Pt(thpy)(bis\text{-NHC})]^+$ are computed in dichloromethane.

Table 3 Calculated $S_1 \rightarrow S_0$ radiative decay rate (k_f) and $S_1 \rightarrow T_n$ ISC rate (k_{ISC}) for $[Pt(thpy)X]^+$ in acetonitrile. The last row gives the observed rate constants estimated from the time-resolved fluorescence measurements in Table 1 ($k_{ISC} = 1/\tau_{ISC}$)

k / s^{-1}	X = dppm (**Pt1**)	X = dcpm (**Pt6**)	X= *bis*-NHC (**Pt10**)[b]
k_f ($S_1 \rightarrow S_0$)	3.44×10^7	3.13×10^7	3.63×10^7
k_{ISC} ($S_1 \rightarrow T_1$) [a]	5.63×10^5	2.31×10^6	6.55×10^6
k_{ISC} ($S_1 \rightarrow T_2$)	5.15×10^9	2.49×10^{10}	1.43×10^{11}
k_{ISC} ($S_1 \rightarrow T_3$)	4.35×10^9	2.35×10^9	7.55×10^8
k_{ISC} (fs-TRF)	5.99×10^9	1.14×10^{10}	

[a]Since the $S_1 \rightarrow T_1$ ISC process is in the Marcus inverted region, k_{ISC} is computed with nuclear tunnelling taken into account. For computational details, see SI. [b]The values for the $[Pt(thpy)(bis\text{-NHC})]^+$ are computed in dichloromethane.

Let us first look at the $S_1 \rightarrow T_1$ ISC pathway. As depicted in Figure 7, the S_1–T_1 energy gap is rather large ($|\Delta E| > 0.75$ eV) with the reorganization energy $\lambda < |\Delta E|$, i.e., it falls in the Marcus *inverted* region; the computed H_{SOC} for this ISC is less than 10 cm^{-1}, which could be rationalized by noting that (a) both S_1 and T_1 are of similar nature and are derived from the HOMO→LUMO transition. SOC could be effective only between states comprised of molecular orbitals of different orientations; in other words, direct SOC should be negligible between states derived from the same orbitals. Therefore, the calculated SOC matrix elements, H_{SOC}, between the S_1 and T_1 excited states are small, and (b) as mentioned above, the S_1 (and T_1) excited state is mainly of $\pi\pi^*$(thpy) character. The localized nature of $\pi\pi^*$(thpy) configuration state function would render the singlet-triplet energy gap to be large. In effect, if eqn. (2) is used to estimate the k_{ISC} rate, the resulting rate constant would be too slow and not competitive with the $S_1 \rightarrow S_0$ radiative decay (calculated k_f is of the order 10^7 s^{-1}). Even if we used a semi-classical equation which takes into account nuclear tunneling (see SI for computational details), the estimated k_{ISC} ($S_1 \rightarrow T_1$) values are still one to two orders of magnitude smaller than k_f ($S_1 \rightarrow S_0$) (Table 3 and Table S6 in SI) and fluorescence should be observed for all the complexes studied herein. Clearly, this is contradictory to the experimental results, and therefore, it is unlikely that the S_1 excited state directly undergoes ISC to the T_1 excited state without intermediate triplet excited states.

For the $S_1 \rightarrow T_3$ ISC pathway, though the estimated ISC rate is fast (k_{ISC} ($S_1 \rightarrow T_3$) > 10^8 s^{-1}, Table 3 and Table S6 in SI), the S_1–T_3 energy gap (ΔE) is positive in all cases (Table 2 and Table S5 in the SI), i.e., the T_3 excited state lies above

the S_1 excited state, meaning that the $S_1 \rightarrow T_3$ ISC is an activated process, and the reverse ISC (RISC), $T_3 \rightarrow S_1$, should be even faster (Table S7 in SI). Therefore, $S_1 \rightarrow T_3$ is also not the most effective ISC pathway for the S_1 excited state.

On the other hand, although the T_2 excited state is more than 1000 cm^{-1} higher-lying than the S_1 excited state at their ground state geometries, the T_2 potential energy minima are *lower-lying* than their respective S_1 potential energy minima, i.e., $\Delta E(S_1–T_2)$ is negative for all the complexes studied in this section and $S_1 \rightarrow T_2$ ISC is a thermodynamically favorable process (Table 2). For this ISC pathway, as $\lambda > |\Delta E|$, it is in the Marcus "*normal*" region. As depicted in Table 3, k_{ISC} ($S_1 \rightarrow T_2$) values for $[Pt(thpy)X]^+$ complexes are in the order X = *bis*-NHC > dcpm > dppm, a trend that is in agreement with the experimental observations of the relative intensity of the phosphorescence to the fluorescence peaks (I_P/I_F). The theoretically calculated ISC rate constants are also in concordance with the measured singlet decay lifetimes: k_{ISC}: X = dppm < X = dcpm. In particular, the calculated ISC rate constants, k_{ISC} ($S_1 \rightarrow T_2$), for X = dppm and dcpm are in excellent agreements with the observed singlet decay rate obtained from fs-TRF (τ(fs-TRF) ~ $1/k_{ISC}$), lending further support that the fluorescence decay in the time-resolved measurements corresponds to ISC from the S_1 excited state to the T_2 excited state.

Table 4 Major contributions to the T_2 excited state of the $[Pt(thpy)X]^+$ complexes. The results are obtained from SS-PCM TD-B3LYP calculations at their respective optimized T_2 geometries

X	HOMO→LUMO	HOMO→L+1	Δε[a]/eV
dppm	23.2% (24.6%)	65.4% (64.4%)	+0.55 (+0.52)
dcpm	25.9% (27.0%)	62.6% (61.7%)	+0.51 (+0.50)
bis-NHC	25.5%	62.6%	+0.50

[a]Δε is the energy gap between the LUMO and L+1 orbitals. Values outside and inside the parentheses are obtained in CH_2Cl_2 and CH_3CN solutions respectively.

As our calculated ISC rates, $k_{ISC}(S_1 \rightarrow T_2)$, are consistent with the experimental results, we sought to understand what factors contribute to the observed trend, $k_{ISC}(S_1 \rightarrow T_2)$ for $[Pt(thpy)X]^+$: X = dppm < dcpm < *bis*-NHC. First, from Table 2, it could be seen that $|\Delta E| < \lambda$, i.e., this ISC pathway is in the Marcus "normal" region. Hence, the FCWD would be governed by two parameters, ΔE and λ. The T_2 excited state, at its optimized geometry, is mainly derived from the HOMO→L+1 transition, with a substantial contribution from the HOMO→LUMO transition (see Table 4 for % contributions of these two major transitions). The L+1 orbital is localized predominantly on the pyridyl moiety (L+3 at the optimized S_0 geometry in Figure 5 becomes L+1 at the optimized T_2 geometry, see Figure S17 in the SI for the MO surfaces and Table S8 for the % contributions of each fragment). Therefore, the T_2 excited state could be described as $^3\pi\pi^*$(thpy) mixed with ^{3}MLCT ($^3[d\pi(Pt) \rightarrow \pi^*(thpy)]$). Interestingly, as the electron-donating capability of the ligand X increases, dppm < dcpm < *bis*-NHC, ΔE becomes more negative and λ becomes smaller. Hence, the activation energy term, $E_a = (\Delta E + \lambda)^2/4\lambda$, becomes smaller, resulting in faster ISC rate as the process is in the Marcus "normal" region. This trend seems to correlate with the % contributions of the HOMO→LUMO transition to the T_2 excited state (Table 4): X = dppm < dcpm ~ *bis*-NHC. This increase in mixing may probably be due to the decrease in orbital energy gap between the LUMO and L+1 orbitals upon increasing the electron-donating power of the auxiliary ligand X.

Besides the nuclear factor (FCWD), the electronic factor H_{SOC} for the $S_1 \rightarrow T_2$ ISC also increases in the order of X = dppm < dcpm < *bis*-NHC (Table 2). This is due to the fact that stronger electron-donating auxiliary ligand X increases metal contributions to the LUMO and L+1 orbitals such that the square of coefficient of the Pt d-orbital (c_d), c_d^2, follows the order of X = dppm < dcpm ~ *bis*-NHC for LUMO (Table S9). In addition, with a stronger σ- donating auxiliary X = *bis*-NHC, the HOMO/H–1 energy gap becomes small enough to allow the H–1→L transition to have some contributions (~1.5 %) to the T_2 excited state at the optimized S_1 excited state geometry. As the HOMO and H–1 have higher metal character (15–19%, Figure S16) and large c_d coefficients, the SOC so-derived is substantial, leading to enhanced SOC matrix elements between the S_1 and T_2 excited states in the $[Pt(thpy)(bis\text{-}NHC)]^+$ **Pt10** complex (Table 2). Therefore, taken together the FCWD factor and the H_{SOC} factor, the calculated ISC rates for the $S_1 \rightarrow T_2$ transition of the $[Pt(thpy)X]^+$ complexes are in the order X = dppm (~10^9 s^{-1}) < dcpm (~10^{10} s^{-1}) < *bis*-NHC (~10^{11} s^{-1}), which reproduces *quantitatively* the experimental findings.

It is worth mentioning here that although our computed ISC rate constants are in excellent agreement with the experimental data, our computations have not taken into account the dynamic nature of the excited state decay. The structural change during excited state decay is especially important when the vibrational relaxation rate constant is compatible with the ISC rate constant. That is, the three parameters, ΔE, λ, and H_{SOC} may be continuously changing upon structural relaxation of the S_1 excited state. The good agreements of our calculations with the experimental data may imply that ΔE and λ vary only slightly upon vibrational relaxation and Condon approximation is a good approximation in evaluating H_{SOC}.

Rationalization of The Excitation Wavelength Dependent ISC. Very often, photoluminescence of most reported organometallic complexes obeys Kasha-Vavilov's rule and the emission is usually independent of the excitation wavelength (λ_{ex}).[48] However, it has been shown in the present work that $[Pt(thpy)(P\hat{}P)]^+$ complexes exhibit excitation wavelength dependent emission spectra. Taking **Pt1** as an example, although TDDFT calculations showed that $S_0 \rightarrow S_2$ excitation peaks at λ < 340 nm, the 0-0 energy of the optimized S_2 excited state was found to be at λ = 365 nm. Thus, upon photo-excitation at λ_{exc} = 350 nm, the S_2 excited

state could be populated, albeit with a low population as reflected in the low absorptivity at λ = 340–350 nm, possibly due to small vibrational overlap between the vibrational ground states of the S_2 and S_0 excited states. As depicted in Table S3 (SI), the S_2 excited state is mainly derived from H-2→LUMO (96%) transition and H-2 has substantial metal character (80% d_{z^2}; see Figure S16 in the SI for the MO surfaces), rendering the S_2 excited state being mainly of ^{1}MLCT character. Contrary to the S_1 excited state which only has one lower-lying triplet excited state (T_1), the S_2 excited state has nine lower-lying triplet excited states. SOC matrix element calculations between S_2 and lower-lying T_m excited states revealed that $\langle S_2|H_{SOC}|T_m\rangle^2$ are much larger (of the order 10^5 cm^{-2} for m = 1–3; see Table S10). Employing eq. (2), the calculated $k_{ISC}(S_2\rightarrow T_2)$ and $k_{ISC}(S_2\rightarrow T_3)$ are respectively 3.82×10^{13} and 1.08×10^{14} s^{-1}, much faster than the $S_2\rightarrow S_1$ internal conversion which is typically in the picosecond time regime (~10^{12} s^{-1}). Thus, the ultrafast ISC from the S_2 excited state to the triplet manifold is the most likely cause of deviation from Kasha-Vavilov's rule and the observed excitation wavelength dependent ISC ($S_2\rightarrow T_m\rightarrow T_1$), as illustrated in Figure 6.

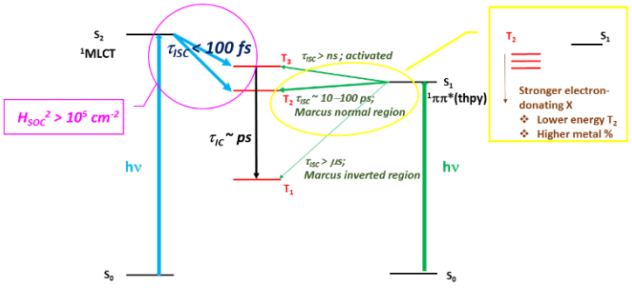

Figure 6. A Jablonski diagram showing relevant optical processes and time constants for the [Pt(thpy)X]$^+$ complexes investigated in this work.

Comparisons between [Pt(ppy)X]$^+$ and [Pt(thpy)]$^+$.

In the present work, all the ppy-bearing Pt(II) complexes **Pt11-Pt14** display predominant phosphorescence. It is thus also of interest to decipher why changing a chromophoric ligand leads to different auxiliary ligand effects on the photo-physical properties, *viz.*, the ISC efficiency is barely affected by the choice of the auxiliary ligand. DFT/TDDFT computations were also performed on two examples, thpy-bearing **Pt5** and ppy-bearing **Pt11**, both with the same auxiliary ligand, dppbz. Figure S18 and S19 depict the frontier MO surfaces and their associated MO energies for **Pt5** and **Pt11** at their respective optimized ground state geometries. The H–2, H–1, HOMO, and LUMO are of the same nature for both complexes, but the HOMO energy of **Pt11** is lower by ~0.3 eV due to its larger metal character (18% for **Pt11** *vs* 10% for **Pt5**) while the other frontier MO energies differ by less than 0.1 eV. As such, there is a profound influence on the excited state ordering (Table S12 and S13), and hence, $\Delta E(S_1–T_n)$ energy gap and the associated SOC matrix element (Table S14). For **Pt5**, similar to the thpy-bearing **Pt1**, only T_1 excited state is lower-lying than the S_1 excited state and the $|\Delta E(S_1–T_1)|$ gap is also quite large (> 7000 cm^{-1}); in addition, both the S_1 and T_1 excited states are of similar nature (dominantly HOMO→LUMO transition), thus resulting in a small SOC matrix element ($H_{SOC}^2 \sim 7$ cm^{-2}); T_2 and T_3 excited states, though having a larger SOC matrix element with the S_1 excited state ($H_{SOC}^2 \sim 3.46 \times 10^2$ and 3.08×10^3 cm^{-2} respectively) due to the participation of ^{3}MLCT states with large metal character (> 35%), are more than 1000 cm^{-1} higher in energy than the S_1 excited state. In contrast, for ppy-bearing complex **Pt11**, there is a close-lying triplet excited state (T_2) to the S_1 excited state ($|\Delta E(S_1–T_2)|$ = 203 cm^{-1}). The T_2 state is mainly of ^{3}MLCT nature (with metal character of H–2 and H–1 of 37 and 47% respectively), thus the SOC matrix element is large ($H_{SOC}^2 \sim 3.47 \times 10^3$ cm^{-2}). T_3 excited state, though higher in energy than the S_1 excited state, is thermally accessible as $|\Delta E(S_1–T_2)|$ = 363 cm^{-1}; the SOC is even larger (H_{SOC}^2 of the order 10^5 cm^{-2}). As is seen in the cases of **Pt1**, **Pt6**, and **Pt10**, changing the auxiliary ligand only changes the $|\Delta E(S_1–T_m)|$ by ~ 0.04 eV (< 400 cm^{-1}) and the SOC increases with more electron-donating auxiliary ligand; it is thus perceived that the auxiliary ligand in the ppy-bearing Pt(II) complexes also fine tunes the $S_1–T_2$ and $S_1–T_3$ energy gap by a similar amount with and the SOC increases with more electron-donating auxiliary ligand. As such, changing the auxiliary ligand of the ppy-bearing Pt(II) complexes still lead to the coupling singlet-triplet energy gap to remain small (< 1000 cm^{-1}). while the SOC matrix element remains large. Therefore, the ISC rate is much faster in the ppy-bearing complexes and predominant phosphorescence observed with little auxiliary ligand effect on the emission properties.

CONCLUSIONS

In this work, we present the photo-physics of [Pt(thpy)X]$^+$ complexes having different auxiliary ligand X, ranging from π-accepting phenylphosphine to σ-donating N-heterocyclic carbene. Though the auxiliary ligand X is not directly involved in the emitting excited state as the chromophore thpy is, it still exerts inductive effect on the Pt(II) ion, which alters the ISC efficiency of this series of Pt(II) complexes. Specifically, increasing the electron-donating ability of the auxiliary ligand X increases the ISC rate, $k_{ISC}(S_1\rightarrow T_2)$. Recently, Karttunen, Chou, and Koshevoy also demonstrated similar findings in a series of gold(I) alkynyl-diphoshpine complexes and attributed this to the greater participation of the d_π orbitals to the *occupied* orbitals of the lowest-lying excited state based on their computational results without explicit calculations on the ISC rate constants.[6] Herein, we have computed the ISC rate constants for the $S_1\rightarrow T_m$ processes and *excellent quantitative* agreement with the fs-TRF measurements has been obtained, giving credibility to our theoretical rationales in the enhanced ISC efficiency with electron-donating dcpm and NHC auxiliary ligands. Our computational results revealed that with more electron-donating auxiliary ligand X, *both occupied and virtual orbitals have higher metal d-orbital contributions and smaller orbital energy* gap, leading to an increase in both FCWD and SOC between the S_1 and T_2 excited states. Thus, the observed ISC is ascribed to $S_1\rightarrow T_2$

ISC through direct SOC in the Marcus "normal" region; the fastest ISC could thus be realized by having the adiabatic singlet-triplet gap close to the reorganization energy, i.e., in the Marcus "activation-less" region (**Figure 7**). In other words, if the activation energy, $E_a = (\Delta E + \lambda)^2/4\lambda$, at the optimized S_1 geometry is close to zero, the rate of $S_1 \rightarrow T_m$ k_{ISC} would only be determined by SOC between S_1 and T_m excited states.

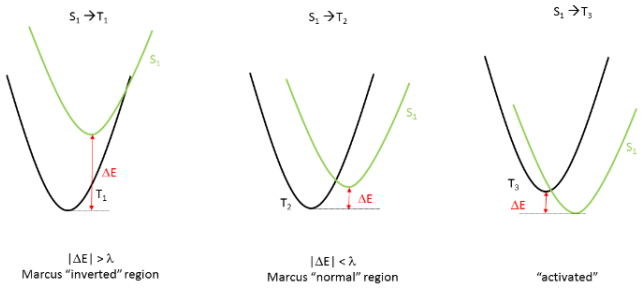

Figure 7. Schematic representations of the $S_1 \rightarrow T_n$ ISC (n = 1–3) within the Marcus electron transfer description.

In addition, it has been shown here that the ISC efficiency of the $[Pt(thpy)X]^+$ complex could be enhanced by using shorter excitation wavelengths. TDDFT calculations revealed that *higher-lying singlet excited states have substantial MLCT character and hence large SOC between the* ^{1}*MLCT (S_2) excited state and the triplet manifold, leading to ultrafast ISC from $S_2 \rightarrow T_m \rightarrow T_1$ ($k_{ISC} > 10^{13}\ s^{-1}$).* Such an interpretation has also been proposed by other groups but without theoretical explanations as to why Kasha-Vavilov's rule is violated.[5,15,20,49] Here, our calculated k_{ISC} for the $S_2 \rightarrow T_2$ and $S_2 \rightarrow T_3$ ISC processes (more than $10^{13}\ s^{-1}$), both of which are faster than $S_2 \rightarrow S_1$ internal conversion, gives strong support the observed excitation-wavelength dependent ISC efficiency.

ASSOCIATED CONTENT

Supporting Information

The Supporting Information is available free of charge via the Internet at http://pubs.acs.org.

Experimental details, synthesis and structural characterization, crystal data and selected parameters, supporting absorption and emission spectra of all complexes in various states, computational methods and results

Accession Codes

CCDC 1518164–1518168, 1998092, 1998096, 1998265-1998269 contain the supplementary crystallographic data for this paper. These data can be obtained free of charge via www.ccdc.cam.ac.uk/data_request/cif, or by emailing data_request@ccdc.cam.ac.uk.

AUTHOR INFORMATION

Corresponding Authors

*E-mail: tongsm@hku.hk (G.S.M.T.)
*E-mail: cmche@hku.hk (C.-M.C.)

ORCID

Kai Li: 0000-0002-5869-1006
Chi-Ming Che: 0000-0002-2554-7219
Glenna So Ming Tong: 0000-0003-3740-2305

Notes

The authors declare no competing financial interest.

ACKNOWLEDGMENT

This work was supported by the Science and Technology Innovation Commission of Shenzhen Municipality (JCYJ20160229123546997, JCYJ20170412140251576), the Major Program of Guangdong Basic and Applied Research (2019B030302009), and National Natural Science Foundation of China (21473114 and 21801170). K.L. acknowledges the support from the Department of Science and Technology of Guangdong Province (2019QN01C617). G.S.M.T acknowledges the research computing facilities and/or advisory services offered by Information Technology Services, the University of Hong Kong. D.L.P. acknowledges the University Development Fund grant 2014–15 for the "New Ultrafast Spectroscopy Experiments for Shared Facilities" from the University of Hong Kong.

REFERENCES

(1) Hudson, Z. M.; Zhao, S.-B.; Wang, R.-Y.; Wang, S. Switchable Ambient-Temperature Singlet–Triplet Dual Emission in Nonconjugated Donor–Acceptor Triarylboron–Pt^{II} Complexes. *Chem. Eur. J.* **2009**, *15*, 6131-6137.
(2) Liu, Y.; Guo, H.; Zhao, J. Ratiometric luminescent molecular oxygen sensors based on uni-luminophores of C^N Pt(II)(acac) complexes that show intense visible-light absorption and balanced fluorescence/phosphorescence dual emission. *Chem. Commun.* **2011**, *47*, 11471-11473.
(3) Yoshihara, T.; Yamaguchi, Y.; Hosaka, M.; Takeuchi, T.; Tobita, S. Ratiometric Molecular Sensor for Monitoring Oxygen Levels in Living Cells. *Angew. Chem. Int. Ed.* **2012**, *51*, 4148-4151.
(4) Geist, F.; Jackel, A.; Winter, R. F. Ligand Based Dual Fluorescence and Phosphorescence Emission from BODIPY Platinum Complexes and Its Application to Ratiometric Singlet Oxygen Detection. *Inorg. Chem.* **2015**, *54*, 10946-10957.
(5) Irmler, P.; Winter, R. F. Complexes trans-Pt(BODIPY)X(PEt_3)$_2$: excitation energy-dependent fluorescence and phosphorescence emissions, oxygen sensing and photocatalysis. *Dalton Trans.* **2016**, *45*, 10420-10434.
(6) Kondrasenko, I.; Chung, K.-y.; Chen, Y.-T.; Koivistoinen, J.; Grachova, E. V.; Karttunen, A. J.; Chou, P.-T.; Koshevoy, I. O. Harnessing Fluorescence versus Phosphorescence Ratio via Ancillary Ligand Fine-Tuned MLCT Contribution. *J. Phys. Chem. C* **2016**, *120*, 12196-12206.
(7) Gupta, S. K.; Haridas, A.; Choudhury, J. Remote Terpyridine Integrated NHC–Ir^{III} Luminophores as Potential Dual-Emissive Ratiometric O_2 Probes. *Chem. Eur. J.* **2017**, *23*, 4770-4773.
(8) Choung, K. S.; Marroquin, K.; Teets, T. S. Cyclometalated iridium–BODIPY ratiometric O_2 sensors. *Chem. Sci.* **2019**, *10*, 5124-5132.
(9) Chergui, M. Ultrafast Photophysics of Transition Metal Complexes. *Acc. Chem. Res.* **2015**, *48*, 801-808.
(10) Cannizzo, A.; van Mourik, F.; Gawelda, W.; Zgrablic, G.; Bressler, C.; Chergui, M. Broadband Femtosecond Fluorescence Spectroscopy of $[Ru(bpy)_3]^{2+}$. *Angew. Chem. Int. Ed.* **2006**, *45*, 3174-3176.
(11) Cannizzo, A.; Blanco-Rodríguez, A. M.; El Nahhas, A.; Šebera, J.; Záliš, S.; Vlček, A.; Chergui, M. Femtosecond Fluorescence and Intersystem Crossing in Rhenium(I) Carbonyl–Bipyridine Complexes. *J. Am. Chem. Soc.* **2008**, *130*, 8967-8974.

(12) Flynn, D. C.; Ramakrishna, G.; Yang, H.-B.; Northrop, B. H.; Stang, P. J.; Goodson, T. Ultrafast Optical Excitations In Supramolecular Metallacycles with Charge Transfer Properties. *J. Am. Chem. Soc.* **2010**, *132*, 1348-1358.
(13) Tong, G. S. M.; Chow, P. K.; Che, C.-M. Where is the Heavy-Atom Effect? Role of the Central Ligand in Tetragold(I) Ethynyl Complexes. *Angew. Chem. Int. Ed.* **2010**, *49*, 9206-9209.
(14) Steffen, A.; Tay, M. G.; Batsanov, A. S.; Howard, J. A. K.; Beeby, A.; Vuong, K. Q.; Sun, X.-Z.; George, M. W.; Marder, T. B. 2,5-Bis(p-R-arylethynyl)rhodacyclopentadienes Show Intense Fluorescence: Denying the Presence of a Heavy Atom. *Angew. Chem. Int. Ed.* **2010**, *49*, 2349-2353.
(15) Hsu, C.-C.; Lin, C.-C.; Chou, P.-T.; Lai, C.-H.; Hsu, C.-W.; Lin, C.-H.; Chi, Y. Harvesting Highly Electronically Excited Energy to Triplet Manifolds: State-Dependent Intersystem Crossing Rate in Os(II) and Ag(I) Complexes. *J. Am. Chem. Soc.* **2012**, *134*, 7715-7724.
(16) Bräm, O.; Messina, F.; Baranoff, E.; Cannizzo, A.; Nazeeruddin, M. K.; Chergui, M. Ultrafast Relaxation Dynamics of Osmium–Polypyridine Complexes in Solution. *J. Phys. Chem. C* **2013**, *117*, 15958-15966.
(17) Nguyen, M.-H.; Wong, C.-Y.; Yip, J. H. K. Ligand Perturbations on Fluorescence of Dinuclear Platinum Complexes of 5,12-Diethynyltetracene: A Spectroscopic and Computational Study. *Organometallics* **2013**, *32*, 1620-1629.
(18) Hung, F.-F.; To, W.-P.; Zhang, J.-J.; Ma, C.; Wong, W.-Y.; Che, C.-M. Water-Soluble Luminescent Cyclometalated Gold(III) Complexes with cis-Chelating Bis(N-Heterocyclic Carbene) Ligands: Synthesis and Photophysical Properties. *Chem. Eur. J.* **2014**, *20*, 8604-8614.
(19) Lin, C.-J.; Chen, C.-Y.; Kundu, S. K.; Yang, J.-S. Unichromophoric Platinum-Acetylides That Contain Pentiptycene Scaffolds: Torsion-Induced Dual Emission and Steric Shielding of Dynamic Quenching. *Inorg. Chem.* **2014**, *53*, 737-745.
(20) Shafikov, M. Z.; Kozhevnikov, D. N.; Bodensteiner, M.; Brandl, F.; Czerwieniec, R. Modulation of Intersystem Crossing Rate by Minor Ligand Modifications in Cyclometalated Platinum(II) Complexes. *Inorg. Chem.* **2016**, 55, 7457-7466.
(21) Sinha, N.; Stegemann, L.; Tan, T. T. Y.; Doltsinis, N. L.; Strassert, C. A.; Hahn, F. E. Turn-On Fluorescence in Tetra-NHC Ligands by Rigidification through Metal Complexation: An Alternative to Aggregation-Induced Emission. *Angew. Chem. Int. Ed.* **2017**, *56*, 2785-2789.
(22) Bachmann, M.; Blacque, O.; Venkatesan, K. Harnessing White-Light Luminescence via Tunable Singlet- and Triplet- Derived Emissions Based on Gold(III) Complexes. *Chem. Eur. J.* **2017**, *23*, 9451-9456.
(23) McCain, J.; Colón, K. L.; Barrett, P. C.; Monro, S. M. A.; Sainuddin, T.; Roque Iii, J.; Pinto, M.; Yin, H.; Cameron, C. G.; McFarland, S. A. Photophysical Properties and Photobiological Activities of Ruthenium(II) Complexes Bearing π-Expansive Cyclometalating Ligands with Thienyl Groups. *Inorganic Chemistry* **2019**, *58*, 10778-10790.
(24) Ai, P.; Mauro, M.; Danopoulos, A. A.; Muñoz-Castro, A.; Braunstein, P. Dual Emission of a Cyclic Hexanuclear Gold(I) Complex. Interplay between Au_3 and Au_2 Ligand-Supported Luminophores. *The Journal of Physical Chemistry C* **2019**, *123*, 915-921.
(25) Blanco-Rodríguez, A. M.; Kvapilová, H.; Sýkora, J.; Towrie, M.; Nervi, C.; Volpi, G.; Záliš, S.; Vlček, A. Photophysics of Singlet and Triplet Intraligand Excited States in [$ReCl(CO)_3$(1-(2-pyridyl)-imidazo[1,5-α]pyridine)] Complexes. *J. Am. Chem. Soc.* **2014**, *136*, 5963-5973.
(26) Chao, H.-Y.; Lu, W.; Li, Y.; Chan, M. C. W.; Che, C.-M.; Cheung, K.-K.; Zhu, N. Organic Triplet Emissions of Arylacetylide Moieties Harnessed through Coordination to $[Au(PCy_3)]^+$. Effect of Molecular Structure upon Photoluminescent Properties. *J. Am. Chem. Soc.* **2002**, *124*, 14696-14706.
(27) Ma, C.; Chan, C. T.-L.; Kwok, W.-M.; Che, C.-M. Ligand [small pi]-conjugation dictated intersystem crossing in phenyleneethynylene gold(I) complexes. *Chem. Sci.* **2012**, *3*, 1883-1892.
(28) Lu, W.; Kwok, W.-M.; Ma, C.; Chan, C. T.-L.; Zhu, M.-X.; Che, C.-M. Organic Triplet Excited States of Gold(I) Complexes with Oligo(o- or m-phenyleneethynylene) Ligands: Conjunction of Steady-State and Time-Resolved Spectroscopic Studies on Exciton Delocalization and Emission Pathways. *J. Am. Chem. Soc.* **2011**, *133*, 14120-14135.
(29) Chang, Y.-C.; Tang, K.-C.; Pan, H.-A.; Liu, S.-H.; Koshevoy, I. O.; Karttunen, A. J.; Hung, W.-Y.; Cheng, M.-H.; Chou, P.-T. Harnessing Fluorescence versus Phosphorescence Branching Ratio in (Phenyl)n-Bridged (n = 0–5) Bimetallic Au(I) Complexes. *J. Phys. Chem. C* **2013**, *117*, 9623-9632.
(30) Koshevoy, I. O.; Lin, C.-L.; Hsieh, C.-C.; Karttunen, A. J.; Haukka, M.; Pakkanen, T. A.; Chou, P.-T. Synthesis, characterization and photophysical properties of PPh_2–C_2–$(C_6H_4)_n$–C_2–PPh_2 based bimetallic Au(I) complexes. *Dalton Trans.* **2012**, *41*, 937-945.
(31) Lam, Y. C.; Gray, H. B.; Winkler, J. R. Intersystem Crossing in Diplatinum Complexes. *J. Phys. Chem. A* **2016**, *120*, 7671-7676.
(32) Monni, R.; Capano, G.; Auböck, G.; Gray, H. B.; Vlček, A.; Tavernelli, I.; Chergui, M. Vibrational coherence transfer in the ultrafast intersystem crossing of a diplatinum complex in solution. *Proc. Natl. Acad. Sci.* **2018**, *115*, E6396-E6403.
(33) Chou, P.-T.; Chi, Y.; Chung, M.-W.; Lin, C.-C. Harvesting luminescence via harnessing the photophysical properties of transition metal complexes. *Coord. Chem. Rev.* **2011**, *255*, 2653-2665.
(34) Kozhevnikov, D. N.; Kozhevnikov, V. N.; Ustinova, M. M.; Santoro, A.; Bruce, D. W.; Koenig, B.; Czerwieniec, R.; Fischer, T.; Zabel, M.; Yersin, H. Synthesis of Cyclometallated Platinum Complexes with Substituted Thienylpyridines and Detailed Characterization of Their Luminescence Properties. *Inorg. Chem.* **2009**, *48*, 4179-4189.
(35) Kozhevnikov, D. N.; Kozhevnikov, V. N.; Shafikov, M. Z.; Prokhorov, A. M.; Bruce, D. W.; Gareth Williams, J. A., Phosphorescence vs Fluorescence in Cyclometalated Platinum(II) and Iridium(III) Complexes of (Oligo)thienylpyridines. *Inorg. Chem.* **2011**, *50*, 3804-3815.
(36) Lai, S.-W.; Chan, M. C.-W.; Peng, S.-M.; Che, C.-M. Self-Assembly of Predesigned Trimetallic Macrocycles Based on Benzimidazole as Nonlinear Bridging Motifs: Crystal Structure of a Luminescent Platinum(II) Cyclic Trimer. *Angew. Chem. Int. Ed.* **1999**, *38*, 669-671.
(37) Zou, T.; Lok, C.-N.; Fung, Y. M. E.; Che, C.-M. Luminescent organoplatinum(II) complexes containing bis(N-heterocyclic carbene) ligands selectively target the endoplasmic reticulum and induce potent photo-toxicity. *Chem. Commun.* **2013**, *49*, 5423-5425.
(38) DePriest, J.; Zheng, G. Y.; Woods, C.; Rillema, D. P.; Mikirova, N. A.; Zandler, M. E. Structure, physical and photophysical properties of platinum(II) complexes containing 7,8-benzoquinoline and various bis(diphenylphosphine) ligands. *Inorg. Chim. Acta* **1997**, *264*, 287-296.
(39) Aghakhanpour, R. B.; Nabavizadeh, S. M.; Rashidi, M.; Kubicki, M. Luminescence properties of some monomeric and dimeric cycloplatinated(II) complexes containing biphosphine ligands. *Dalton Trans.* **2015**, *44*, 15829-15842.
(40) Solomatina, A. I.; Su, S.-H.; Lukina, M. M.; Dudenkova, V. V.; Shcheslavskiy, V. I.; Wu, C.-H.; Chelushkin, P. S.; Chou, P.-T.; Koshevoy, I. O.; Tunik, S. P. Water-soluble cyclometalated platinum(II) and iridium(III) complexes: synthesis, tuning of the photophysical properties, and in vitro and in vivo phosphorescence lifetime imaging. *RSC Adv.* **2018**, *8*, 17224-17236.
(41) Li, K.; Cheng, G.; Ma, C.; Guan, X.; Kwok, W.-M.; Chen, Y.; Lu, W.; Che, C.-M. Light-emitting platinum(II) complexes supported by tetradentate dianionic bis(N-heterocyclic carbene) ligands: towards robust blue electrophosphors. *Chem. Sci.* **2013**, *4*, 2630-2644.

(42) Cheng, G.; Kui, S. C. F.; Ang, W.-H.; Ko, M.-Y.; Chow, P.-K.; Kwong, C.-L.; Kwok, C.-C.; Ma, C.; Guan, X.; Low, K.-H.; Su, S.-J.; Che, C.-M. Structurally robust phosphorescent [Pt(O^N^C^N)] emitters for high performance organic light-emitting devices with power efficiency up to 126 lm W^{-1} and external quantum efficiency over 20%. *Chem. Sci.* **2014**, *5*, 4819-4830.
(43) Chow, P.-K.; Cheng, G.; Tong, G. S. M.; To, W.-P.; Kwong, W.-L.; Low, K.-H.; Kwok, C.-C.; Ma, C.; Che, C.-M. Luminescent Pincer Platinum(II) Complexes with Emission Quantum Yields up to Almost Unity: Photophysics, Photoreductive C-C Bond Formation, and Materials Applications. *Angew. Chem. Int. Ed.* **2015**, *54*, 2084-2089.
(44) Marcus, R. A. Nonadiabatic processes involving quantum - like and classical-like coordinates with applications to nonadiabatic electron transfers. *J. Chem. Phys.* **1984**, *81*, 4494-4500.
(45) Balzani, V.; Juris, A.; Venturi, M.; Campagna, S.; Serroni, S. Luminescent and Redox-Active Polynuclear Transition Metal Complexes. *Chem. Rev.* **1996**, *96*, 759-833.
(46) Beljonne, D.; Shuai, Z.; Pourtois, G.; Bredas, J. L. Spin–Orbit Coupling and Intersystem Crossing in Conjugated Polymers: A Configuration Interaction Description. *J. Phys. Chem. A* **2001**, *105*, 3899-3907.
(47) Brunschwig, B. S.; Sutin, N. Rate-Constant Expressions for Nonadiabatic Electron-Transfer Reactions. *Comments Inorg. Chem.* **1987**, *6*, 209-235.
(48) Turro, N. J.; V., R.; Scaiano, J. C. Modern Molecular Photochemistry of Organic Molecules. *University Science Books*, Sausalito, CA, 2010.
(49) Robson, K. C. D.; Hu, K.; Meyer, G. J.; Berlinguette, C. P. Atomic Level Resolution of Dye Regeneration in the Dye-Sensitized Solar Cell. *J. Am. Chem. Soc.* **2013**, *135*, 1961-1971.

SYNOPSIS TOC. Controlling of ISC rate constant is key to the tailoring of emission properties of transition metal complexes. Both spectroscopic and theoretical studies of a series of cyclometalated Pt(II) complexes reveal that ISC rate can be tuned by varying the electron-donating capability of the auxiliary ligands. Moreover, hyper ISC from higher-lying singlet excited state to triplet manifold has been unveiled by theoretical studies, explaining the excitation wavelength dependent dual fluorescence-phosphorescence emissions for the present Pt(II) complexes.

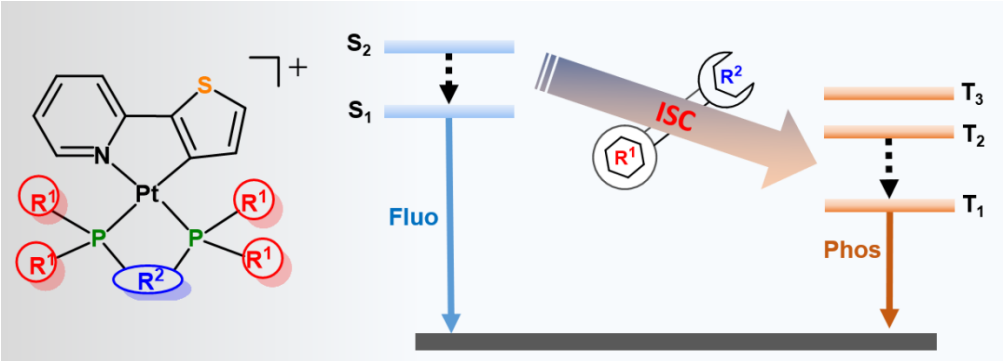

For Table of Contents Only